J Supercond Nov Magn (2014) 27:133–141
DOI 10.1007/s10948-013-2280-7

ORIGINAL PAPER

The Role of Weak Links and Zn-Doping on Magnetic Parameters of High-T_c Superconductors

Ugur Topal · E. Gulce Coker · Fatma Alıkma · Ugur Kolemen · Orhan Uzun

Received: 13 May 2013 / Accepted: 5 June 2013 / Published online: 11 July 2013
© Springer Science+Business Media New York 2013

Abstract The second harmonic signal, which is generated by co-application of AC and DC fields to polycrystalline type-II superconductors, were analyzed in terms of the weak links and the critical current density. With this aim the $YBa_2Cu_{3-x}Zn_xO_{7-y}$ ($x = 0, 0.01, 0.02, 0.03, 0.05$, and 0.1) samples were synthesized in order to adjust intergranular couplings and thus the strength of weak links. The mechanical and magnetic measurements are in good agreement on that Zn doping reduces strength of the links between grains; however, contrary to the common expectations, it has no direct contribution to the 2nd harmonic signal strength.

Keywords Superconductors · Superconductivity · Magnetometer · Magnetic properties

1 Introduction

The magnetic sensors have been very useful for many applications such as space sector, archaeology, medicine, mineral exploration, military, etc. [1]. Since magnetic applications are so varied, the choice of magnetic sensor can be a difficult task. For instance, working range of the sensor must cover 10^{-9}–10^{-4} T for applications in the navigation systems [1]. Similarly, the investigation of local anomalies of the earth field requires measurement capability of magnetic fields in the range of 10^{-5}–10^{-3} T. In order to measure magnetic field signals generated from the ionic current activity of heart muscle, the sensor must have sensitivity to the fields less than 10^{-12} T.

The known technologies used for magnetic field sensing are mainly: search coils, fluxgate, nuclear precession, SQUID, Hall-effect, giant magnetic resistance, fiber optic, and magnetooptic [2]. Thus, for instance, while Hall-effect sensors seems to be suitable for analyzing earth field analysis, SQUID magnetometer and search coil are good candidates for the analysis of the ionic current activity of heart muscles [3–6]. There has been an increased demand for high sensitive magnetic sensors (from pT to μT) for navigation systems and defense applications [7]. In this range, the most popular sensing technology is known to be fluxgate magnetometer (in a range of 10 pT to 0.1 mT) [8, 9]. Another method, which uses polycrystalline high-T_c superconductors instead of ferromagnetic core as in the case of the fluxgate magnetometer, also covers this range with minimum detectable magnetic fields down to 0.5 nT [10, 11]. The working principle is almost the same with the fluxgates; as it is well known that the fluxgates are based on the periodical saturation of a soft ferromagnetic core driven by an AC field [6, 8]. When the core saturates, the external field being measured will have no contribution to the magnetization of the core. On the other hand, when the core goes out of the saturation by decreasing the amplitude of excitation field, magnetization of the core will change by the external field. In these conditions, the voltage induced in the sense coil consists of even harmonics of the excitation frequency.

U. Topal (✉) · F. Alıkma
TÜBİTAK-UME (National Metrology Institute), P.K. 54, 41470 Gebze-Kocaeli, Turkey
e-mail: ugur.topal@tubitak.gov.tr

E.G. Coker
Physics Department, Yeditepe University, Istanbul, Turkey

U. Kolemen
Department of Physics, Faculty of Science and Arts, Gaziosmanpaşa University, 60240 Tokat, Turkey

O. Uzun
Department of Metallurgical Engineering, Faculty of Engineering, Bülent Ecevit University, Zonguldak 67100, Turkey

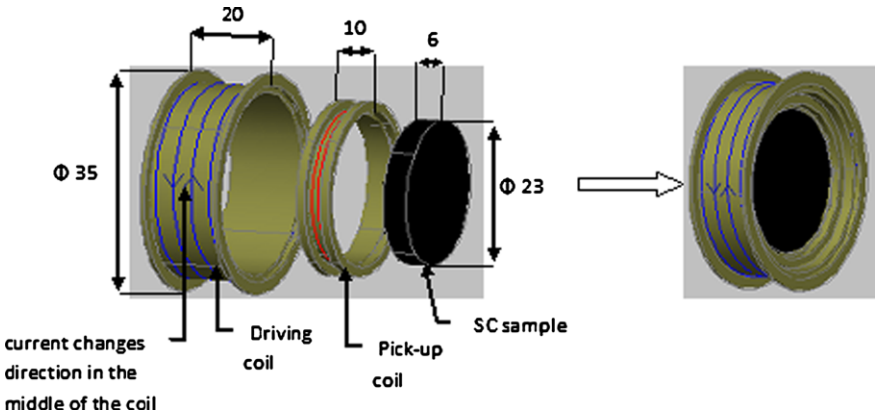


Fig. 1 The coil configuration used in experiments

The sensor using superconductor core is based on nonlinear magnetization of polycrystalline type II superconductors when the core is under both AC and DC fields [12–17]. So, the core is excited by an AC field and the even harmonics are generated due to the external DC magnetic field being measured. The studies have shown that the even harmonic signal changes quite linearly and sharply with DC field.

In literature, the magnetization of a polycrystalline superconductor is known to be through the summation of intergranular and intragranular contributions of circulating supercurrents [18]. At low fields, intergranular regions dominate the sample's magnetization (i.e., the flux first enters to the specimen through intergrain regions rather than intragrain regions). Therefore, the links between grains are required to be weak in order to make quite low flux entries possible and so, to increase DC field sensitivity. A recent work has shown that Zn doping reduces the intergranular couplings [19]. So, it is expected that DC field sensitivity can be improved by Zn doping. With this knowledge, we synthesized the polycrystalline $YBa_2Cu_3O_7$ samples at different concentrations of Zn atoms in order to understand the contribution of the weak links to the second harmonic signal strength. Synthesis conditions (such as furnacing temperatures) and dimensions of the superconducting samples are kept the same just to clarify the role of weak links (to avoid demagnetization factor, etc.). The measurements were supported by mechanical (hardness, elastic modulus) and magnetic measurements (the M–T and the M–H).

2 Experimental

Samples of $YBa_2Cu_{3-x}Zn_xO_{7-y}$ ($x = 0$, 0.01, 0.02, 0.03, 0.05, 0.1), used as sensing elements, were prepared by the conventional solid state reaction method. High purity powders (99.99 %) of Y_2O_3, $BaCO_3$, CuO, and ZnO were weighed in the appropriate amounts and mixed well using an agate mortar. Then the powder was pressed into pellets under pressure of 1400 kgf/cm^2. The pellets, containing different amounts of Zn given above, were calcined at 925 °C for 72 h with intermediate grinding, mixing and pelletizing after each 24 h. Here, it must be noted that all samples were furnaced at same atmospheric conditions in order to minimize the contribution of external factors, and thus, to understand the effects of Zinc doping on second harmonic signal strength. Later, the samples were oxygenated under oxygen flow (0.5 lt/min) by holding at 900 °C (16 h) and 450 °C (24 h). Then the samples were sandpapered to the same dimensions with diameter of 23 mm and thickness of 7 mm to avoid the possible variations coming from the demagnetization factor. The M–T and the M–H measurements were done by using MPMS-5 SQUID magnetometer from Quantum Design. Experimental set up for the second harmonic measurements were described with details in [20, 21].

The coil configurations used in experiments are seen in Fig. 1 (the numbers in drawing are mm). The pick-up coil, which was used for the detection of the second harmonic signal generated by superconducting specimen, has 2100 turns/cm (wire diameter is 100 μm). The driving coil, for applying an AC magnetic field to the superconductor, has 50 turns/cm (wire diameter is 200 μm) and the winding changes direction in the middle of the template. The pick-up coil was moved through the driving coil to minimize mutual inductance between these coils (i.e., mechanical compensation). We must note that the fiber glass was preferred as a template for the coils to minimize thermal expansion in liquid nitrogen.

An electronic filter with high quality factor Q was used to eliminate signals other than $2f = 99.8$ kHz (for details, see [21]). The DC-field was applied by a calibrated solenoid with coil constant of 15.61 Oe/A, which is traceable to primary standards of dimensional and time & frequency over NMR teslameter. The tests were performed at liquid nitrogen temperature and the test place was shielded from surrounding magnetic fields by using trio Mu-metal chambers. For electrical connections, well-screened cables were preferred.

The indentation experiments were conducted with a Berkovich tip using the NH-2 Nanoindenter (manufactured by CETR) with load and displacement resolutions of

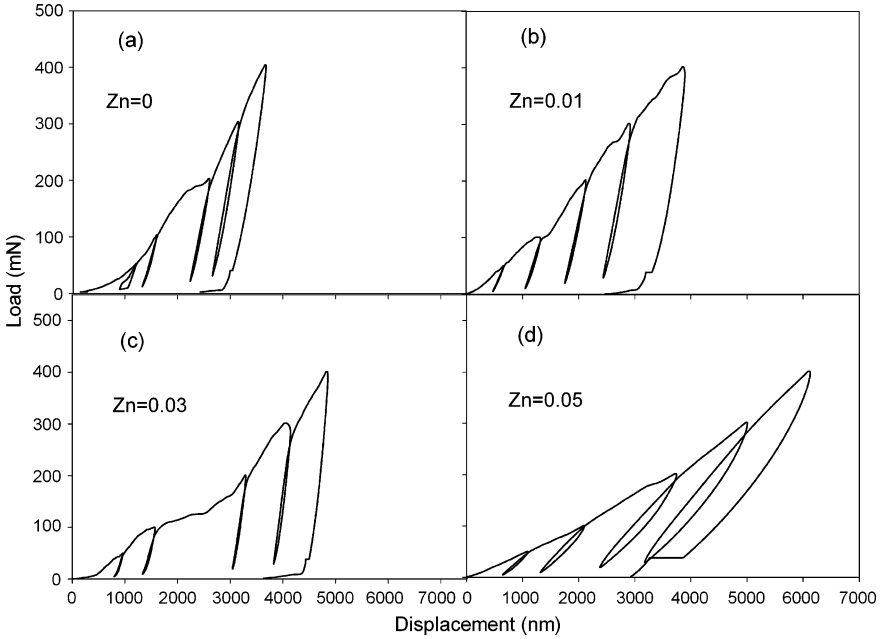


Fig. 2 Typical load-unloading curves for Zn doped and undoped polycrystalline YBaCuO samples

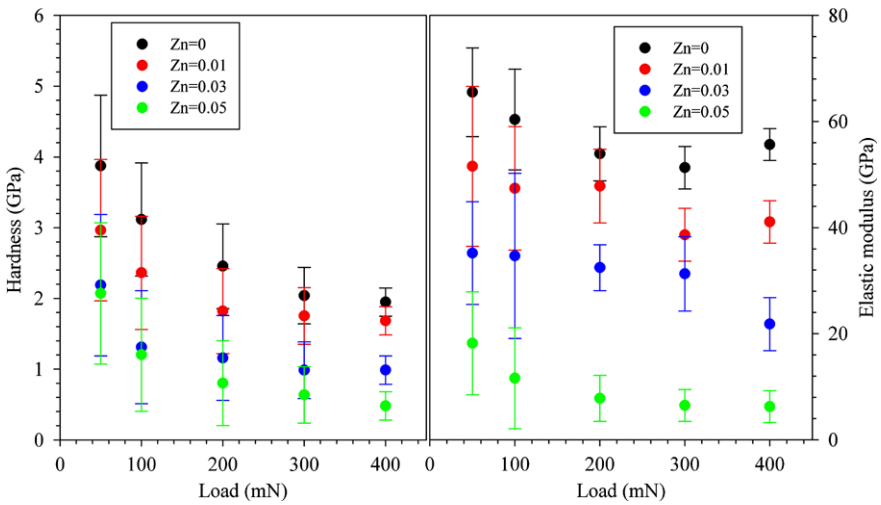


Fig. 3 Variations of the hardness and elastic modulus with the applied load for Zn doped and undoped polycrystalline YBaCuO samples

±0.1 μN and ±0.03 nm, respectively. Before the indentation experiments, the samples on the mounting stage were adjusted to prevent tilting in the z-axis. At least five-step load-unload indentation experiments were carried out at different locations of the samples as the nature of the samples was porous and heterogeneous. Loading steps were adjusted as 50, 100, 200, 300, and 400 mN.

3 Results and Discussion

3.1 Mechanical Measurements

Typical load-unloading curves for the undoped and Zn-doped samples are shown in Fig. 2. The load is cyclically increased from 50 mN to a maximum of 400 mN. The curves demonstrate that all samples show elasto-plastic behavior during indentation. Figure 3 shows the hardness and reduced elastic modulus profiles obtained from the load-unloading curves of the samples. The hardness values were calculated according to the models developed by Oliver Pharr [22]. They are found to be load dependent (ISE; Indentation Size Effect Behavior). It is well known that the microhardness in ceramics is dependent on the load at low loads and independent of the load at higher loads. The measured hardness in our samples decreases rapidly with increasing load up to 200 mN and remains nearly constant for the higher loads. Similar cases were also observed on different superconductor materials [23–25].

As seen from Fig. 3, the hardness of YBaCuO decreases with increasing Zn content. All of the hardness profiles have a great dispersion in its values. Such dispersion can be as-

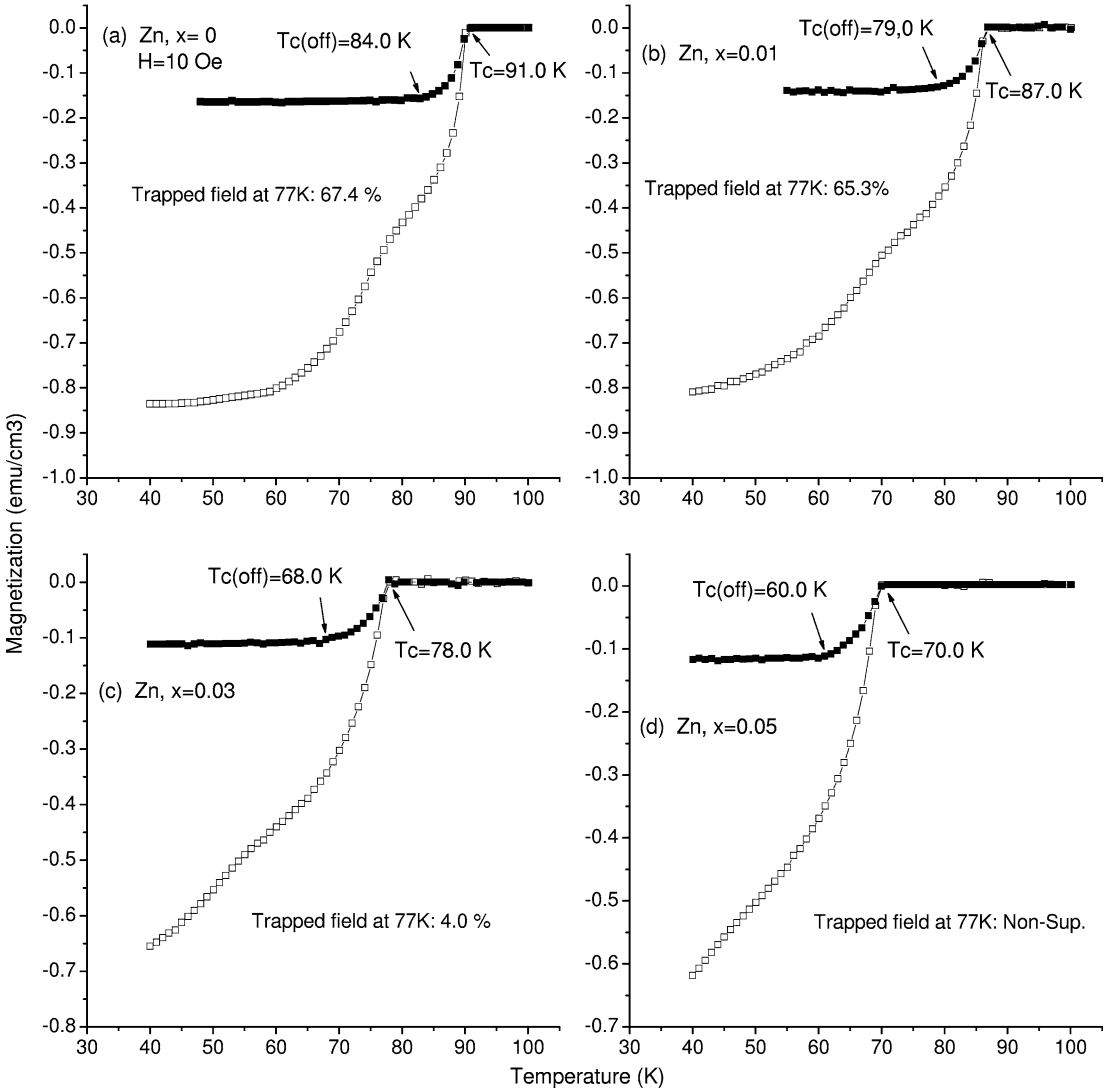


Fig. 4 The M–T curves of Y-123 compounds as a function of Zn content

cribed to the microstructural properties of the studied samples, such as the porosity, bad contact between grains, and the test conditions, such as applied load range [26–34]. The reduced modulus (E_r) vs. the maximum load curves were also shown in Fig. 3. Since the E_r is an intrinsic material property and fundamentally related to atomic bonding, the measured reduced modulus is expected to be constant with indentation depth (or load). The results reveal a small overestimation only at load 50 mN. The measured values of the elastic modulus in the present situation are compatible with the reported data [26, 28–34]. The same tendency was observed for the E_r values of the samples as seen in the H values. That is, it decreases as Zn-concentration increases. In literature, the critical current density J_c was reported to be related with the mechanical properties [35, 36]. The studies on YBCO and BSCCO superconducting systems have shown that the J_c varies proportionally with the mechanical hardness [35]. With this reason, the J_c was expected to take lower values as the Zn-concentration increases, which will be confirmed at further part of the text. It was also reported by Sergius et al. as the mechanical parameters (the H and E_r values) are directly proportional with the intergrain couplings in addition to some other factor, such as porosity [36]. Consequently, we understand that the mechanical measurements confirm our expectations on the weakening of the links between grains as the Zn-addition.

3.2 Magnetic Measurements

The M–T and the M–H curves of Y-123 compounds as a function of Zn content are shown in Figs. 4 and 5, respectively. It is seen that the superconducting transition temperature T_c (on) decreases significantly as Zn concentration increases, which is well agreement with the data published

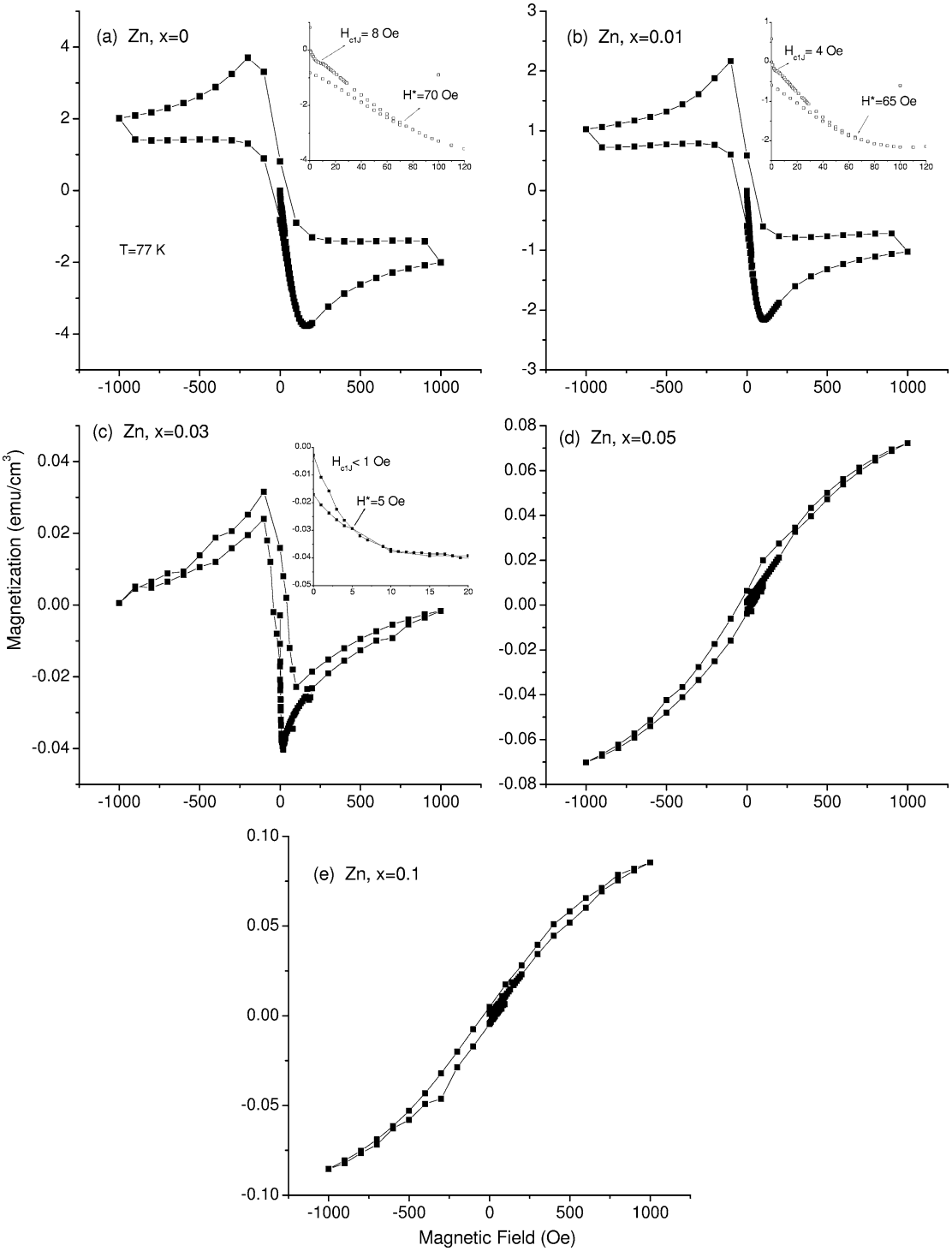


Fig. 5 The M–H curves of Y-123 compounds as a function of Zn content at 77 K with maximum field of 1000 Oe. *Insets*: The magnification of 4th quadrant of the loops

in [19] and attributed to the substitution of Zn atoms for Cu atoms in the CuO_2 planes. For $x = 0.05$, the T_c (on) decreases down to 70 K. The M–T data also reveals that the transition width increases with the increase of Zn content. Since large transition width indicates the presence of weak couplings between grains of ceramic superconductors (SC) [37, 38], it will be correct to state that strength of the links between grains becomes weaker with Zn addition, which also confirms the results of [19] and our mechanical measurements. As known, the trapped field, which is

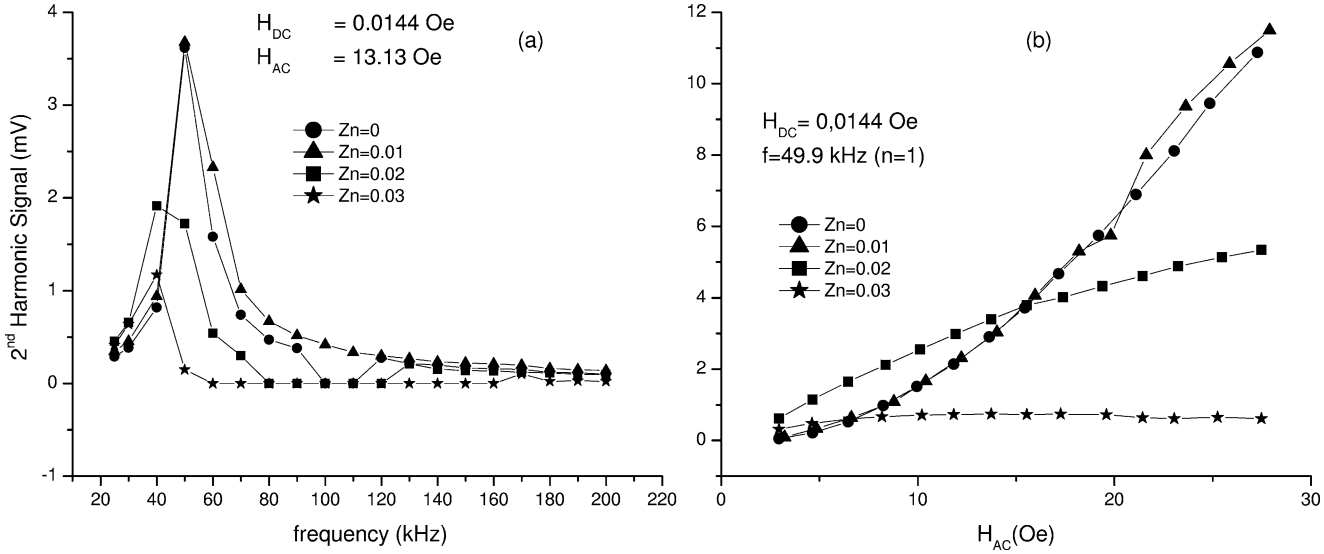


Fig. 6 Dependence of the second harmonic signal on (**a**) driving field frequency and (**b**) driving field amplitudes

the field remaining in SC specimen after removal of applied field, gives us information about strength of pinning force and proportionally magnitude of critical current density J_c. The trapped field at working temperature of 77 K was also determined from the M–T curves and found to be decreasing as Zn content increases. For instance, while the trapped field is ∼4.0 % of applied field for Zn content of $x = 0.03$, it is determined to be 67.4 % for the undoped sample.

The M–H curves at 77 K reveals that magnetic moment corresponding to superconductivity is apparent until Zn concentration of $x = 0.03$, above which ferromagnetic like magnetization becomes visible and dominates the superconductivity. Here, we must note that the amplitude of the second harmonic signal is expressed to be $V_2 \sim \omega H_{\mathrm{DC}} H_{\mathrm{AC}}^3 AN/J_c$ (where A is the effective area and N is the number of turns of the detection coil) [39, 40]. In this formula, the parameters other than the critical current density J_c, such as excitation frequency ω and excitation field amplitude H_{AC}, are not related to properties of the studied samples. However, the J_c is a characteristic parameter of the superconducting specimen, and as well known, takes lower values for the granular samples having weakly coupled grains. With this reason, the J_c values were derived from the M–H loops by using the well-known Bean model [41] and determined to be 290 A/cm^2, 220 A/cm^2, and 7 A/cm^2 at zero field for the undoped, $x = 0.01$ and $x = 0.03$, respectively. As seen, the J_c decreases as the Zn concentration increases. This may also be ascribed to the weakening of the links between grains.

The reason of M–H measurements was also to extract some crucial parameters (H_{1cg}, H^*, $H_{\mathrm{DC}}/H_{\mathrm{AC}}$) required for determination of region where the second harmonic signal changes linearly with the DC-field, which is necessary for feasibility of the sensor. The insets of Fig. 5 show the expanded fourth quadrant of the loops to determine intergrain first critical field H_{c1J} (i.e. the flux starts to penetrate SC specimen through grain boundaries above this field) and the minimum field required for penetration through the entire specimen H^*. Magnetic field corresponding to first deviation from the linearity in initial magnetization curve was accepted to be H_{1cJ}. Crossing point of initial magnetization curve with the M–H loop at the fourth quadrant belongs to H^*. With this approach, the H_{1cJ} and H^* are seen as decreasing sharply with the increase of Zn content. The H_{1cJ} decreases from 8 Oe to less than 1 Oe in case the SC sample is doped with Zn of $x = 0.03$. Similarly, the H^* falls to 5 Oe (from 65 Oe for the undoped one) with the same concentration of Zn.

3.3 The Second Harmonic Measurements

As mentioned before, the magnitude of the harmonic signal is expected to be linearly proportional with frequency ω and H_{AC}^3/H^* if the amplitude of the AC field H_{AC} is larger than H_{1cJ} (where $H^* \sim J_c$). On the other hand, some studies in literature have shown that there are optimal values for both of the parameters since, as known in electronics, such optimal values show variations depending on the coil design [42]. In order to define optimal frequency, a sinusoidal signal was driven to excitation coil by using an ultra low distortion function generator up to a frequency of 200 kHz. The signal amplitude H_{AC} was kept constant at 13.13 Oe. A DC-field of 0.0144 Oe, which is required for the generation of the second harmonic signal, was applied by a calibrated solenoid and the signal induced on detection coil at frequency of $2f$ was monitored by a lock-in amplifier. Figure 6a shows the second harmonic signal vs. the

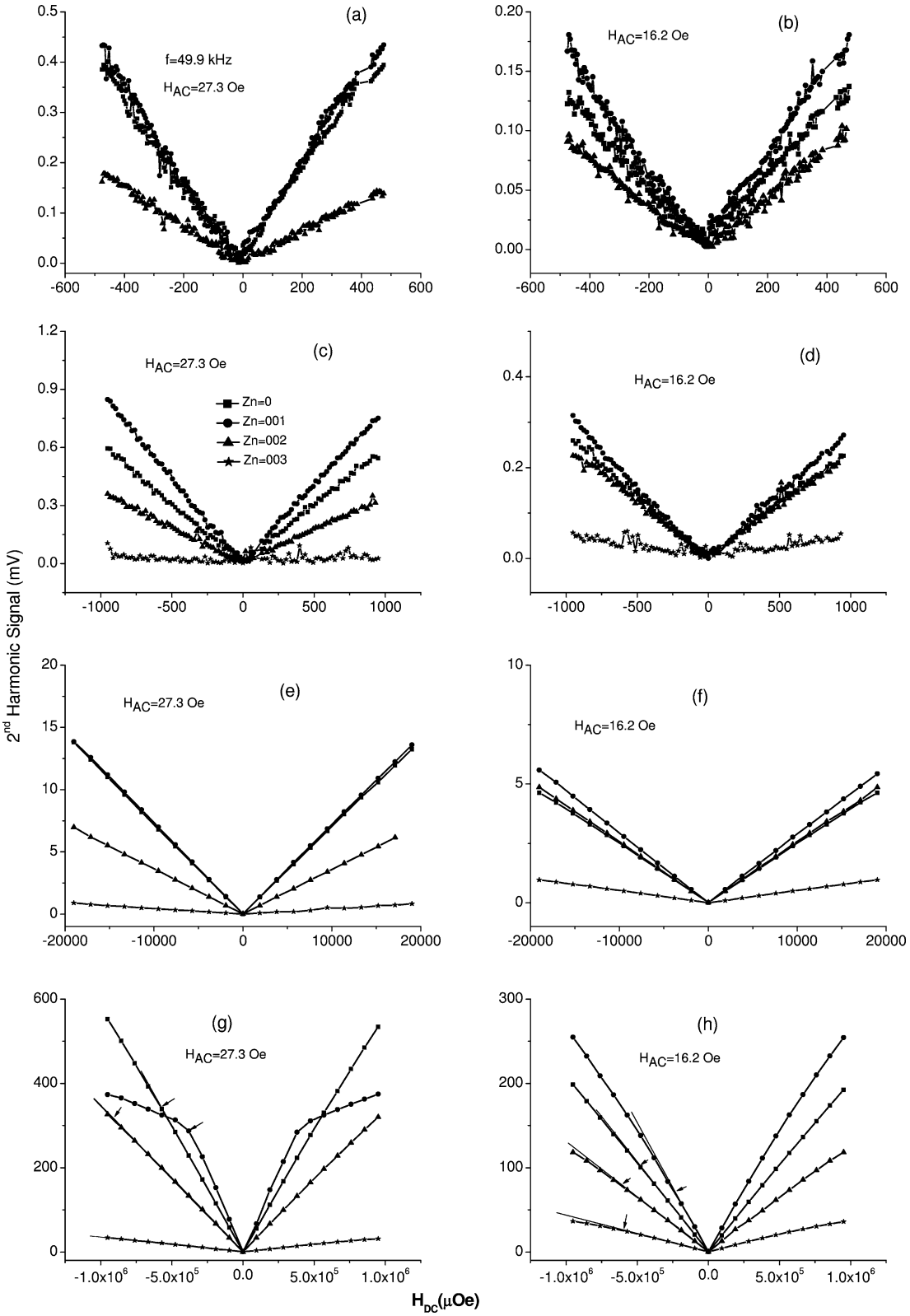


Fig. 7 Variation of the 2nd harmonic amplitude (V_{2f}) for the YBCO pellets as a function of applied DC field at 77 K for AC fields amplitudes of 16.2 Oe and 27.3 Oe

frequency curve of $YBa_2Cu_3O_7$ superconductors with different amounts of Zn atoms. Here, we must note that the measurements were carried out at liquid nitrogen temperature. It is seen that the optimal frequency changes depending on the studied sample since all measurements were realized at same conditions. While it is at 50 kHz for the undoped and $x = 0.01$, it is at 40 kHz for $x = 0.02$ and 0.03. It is also interesting that signal amplitude initially shows a slight increment with Zn doping for $x = 0.01$, but then decreases sharply above this concentration. Optimal AC-field analysis were done at frequency of 49.9 kHz with AC field amplitude between 2.9 Oe and 27.5 Oe (maximum applicable field) and shown in Fig. 6b. As it is seen, the signal strength increases proportionally with the AC field amplitude except for the sample doped with Zn atoms of $x = 0.03$, on which optimal AC field amplitude was determined to be 10.2 Oe.

Figure 7 shows the variation of the second harmonic signal amplitude as a function of DC-field at 77 K and for different scales. The data were gathered for AC fields with amplitudes of 16.2 and 27.3 Oe, and at a frequency of 49.9 kHz ($n = 1$). The strength of the second harmonic signal is larger for higher AC field amplitudes, but not changes linearly with H_{AC}^3 as stated in the second harmonic formula given above. Besides, the experiments realized in high amplitude of AC-field reveal better sensitivity to DC-field (see Figs. 7a and 7b). These experiments have shown that the highest signal strength was observed in the Zn-doped sample with $x = 0.01$. However, further increase of Zn concentration adversely affect the signal strength, which takes values more than one-tenth of the sample with $x = 0.01$ for the sample with $x = 0.03$. The data of the Zn-doped sample with $x = 0.01$ seems also less noisy, especially at high AC fields, compared to the others. Experiments with DC-field steps of 0.5 nT (Figs. 7a–b) and 2 nT (Fig. 7c–d) reveal that 2 nT can be detected by using the sample with Zn content of $x = 0.01$.

Similar to our experimental results seen on H_{AC} dependence of V_2, the J_c dependence of 2nd harmonic signal also departs from the proposed relation of $V_2 \sim \omega H_{DC} H_{AC}^3 AN/J_c$. If we accept that this formula is correct, then the sample with low J_c (it is the Zn-doped sample with $x = 0.03$ in present case) must result in higher signal strength. As a result, it seems to be incorrect to make such a generalization.

To determine the working range of the sensor, the experiments were also realized at large DC-field intervals (Fig. 7e–h). The deviation from the linearity was accepted to be the upper limit of the sensor (marked with arrows in the Fig. 7). The upper limits are 0.38 Oe, 0.57 Oe, 0.91 Oe, and 1.06 Oe for the $x = 0.01$, the undoped, $x = 0.02$ and $x = 0.03$, respectively. The maximum values of the H_{DC}/H_{AC} ratios, above which nonlinearity on DC-field dependence of 2nd harmonic signal is observed, were determined to be 0.014, 0.021, 0.033, and 0.038 for the same order of the samples. As it is seen, the most sensitive one to DC fields has less the upper limit. So, it provides us with the opportunity to choose desired working range depending on our usage purpose. Besides, the transfer functions (dV/dB) were determined to be 7590 V/T, 5940 V/T, 3450 V/T, and 350 V/T for the $x = 0.01$, the undoped, $x = 0.02$ and $x = 0.03$, respectively. It means that much lower DC fields can be detected if the noises coming from the external factors, such as; the coil, the core geometry, and the main line, are suppressed. The detailed analysis of such kind of noises will be subject of our future works.

4 Conclusion

In this work, the effect of weak links between the grains of YBaCuO ceramics on the strength of the second harmonic signal was examined. Contrary to the expectations of literature, there is no direct relationship between the signal strength and the weak links. Experiments carried out on a series of Zn-doped YBaCuO samples, where the J_c values were observed to be decreasing with the increase of Zn concentration, have shown that the highest $2f$ signal corresponds to the at least Zn-doped sample ($YBa_2Cu_{2.99}Zn_{0.01}O_{7-y}$). The 2 nT DC-field could be detected by using this SC specimen as the sensing core. On the other hand, the upper limit takes lower values compared to the less sensitive one.

Acknowledgements This work was supported by the Scientific and Technological Research Council of Turkey (TÜBİTAK) grant no. 109T715.

References

1. Diaz-Michelena, M.: Sensors **9**, 2271 (2009)
2. Rovati, L.: IEEE Trans. Ind. Electron. **59**, 571 (2012)
3. Atalay, S., Yagmur, V., Atalay, F.E., Bayri, N.: J. Magn. Magn. Mater. **323**, 2818 (2011)
4. Stupakov, O.: J. Magn. Magn. Mater. **324**, 631 (2012)
5. Tanaka, S., Hatsukade, Y., Ohtani, T., Suzuki, S.: J. Magn. Magn. Mater. **321**, 880 (2009)
6. Lenz, J., Edelstein, A.S.: IEEE Sens. J. **6**, 631 (2006)
7. Lei, J., Lei, C., Zhou, Y.: Measurement. doi:10.1016/j.measurement.2011.10.013
8. Ripka, P.: Sens. Actuators A, Phys. **33**, 129 (1992)
9. Kaluza, F., Gruger, A., Gruger, H.: Sens. Actuators A, Phys. **106**, 48 (2003)
10. Gallop, J.C., Lilleyman, S., Langham, C.D., Radcliffe, W.J., Stewart, M.: IEEE Trans. Magn. **25**, 896 (1989)
11. Dey, T.K., Chattopadhyay, M.K., Ghatak, S.K.: Sens. Actuators, B, Chem. **55**, 222 (1999)
12. Bean, C.P.: Rev. Mod. Phys. **36**, 31 (1964)
13. Jeffries, C.D., Lam, Q.H., Kim, Y., Kim, C.M., Zettl, A., Klein, M.P.: Phys. Rev. B **39**, 11526 (1989)
14. Shaulov, A., Dorman, D.: Appl. Phys. Lett. **53**, 2680 (1988)
15. Ji, L., Shon, R.H., Spalding, G.C., Lobb, C.J., Tinkham, M., Zhao, Z.X.: Bull. Am. Phys. Soc. **34**, 602 (1989)

16. Xia, T., Stroud, D.: Phys. Rev. B **39**, 4792 (1989)
17. Ji, L., Sohn, R.H., Spalding, G.C., Lobb, C.J., Tinkham, M.: Phys. Rev. B **40**, 10936 (1989)
18. Buckley, J.R., Khare, N., Donaldson, G.B., Cochran, A., Hui, Z.: IEEE Trans. Magn. **27**, 3051 (1991)
19. Liyanawaduge, N.P., Singh, S.K., Kumar, A., Awana, V.P.S., Kishan, H.: J. Supercond. Nov. Magn. **24**, 1599 (2011)
20. Topal, U., Alikma, F., Birlikseven, C.: J. Supercond. & Novel Magn. doi:10.1007/s10948-011-1393-0
21. Alikma, F., Birlikseven, C., Gulmez, G., Turhan, E., Coker, E.G., Topal, U.: J. Supercond. Nov. Magn. (2012). doi:10.1007/s10948-012-1684-0
22. Oliver, W.C., Pharr, G.M.: J. Mater. Res. **7**, 1564–1583 (1992)
23. Güçlü, N., Uzun, O., Kölemen, U.: Mater. Charact. **57**, 166–170 (2006)
24. Kölemen, U., Uzun, O., Aksan, M.A., Güçlü, N., Yakıncı, E.: J. Alloys Compd. **415**, 294–299 (2006)
25. Kölemen, U., Çelebi, S., Karal, H., Öztürk, A., Çevik, U., Nezir, S., Görür, O.: Supercondcuting and Vickers hardness properties of ZnO-added YBCO polycrystalline superconductors. Phys. Status Solidi (b) **241**(2), 274–283 (2004)
26. Poole, C.P.: Handbook of Superconductivity, pp. 577–609. Academic Press, San Diego (2000)
27. Yan, M.F., Ling, H.C., Obryan, H.M., Gallager, P.K., Rhodes, W.W.: Process-related problems of $YBa_2Cu_3O_x$ superconductors. Mater. Sci. Eng. B **1**, 119–129 (1988)
28. Reddy, R.R., Murakami, M., Tanakam, S., Reddy, P.V.: Physica C **257**, 137 (1996)
29. Miyamato, T., Nagashima, K., Sakai, N., Murakami, M.: Supercond. Sci. Technol. **13**, 816 (2000)
30. Yoshino, Y., Iwabuchi, A., Noto, K., Murakami, M.: Physica C **357–360**, 796 (2001)
31. Sakai, S., Seo, S.J., Inoue, K., Myiamoto, T., Murakami, M.: Physica C **335**, 107 (2000)
32. Tancret, F., Monot, I., Osterstock, F.: Mater. Sci. Eng. A **298**, 268 (2001)
33. Matsui, M., Sakai, N., Murakami, M.: Supercond. Sci. Technol. **15**, 1092 (2002)
34. Foerster, C.E., Lima, E., Rodrigues, P. Jr., Serbena, F.C., Lepienski, C.M., Cantão, M.P., Jurelo, A.R., Obradors, X.: Braz. J. Phys. **38**, 341 (2008)
35. Güçlü, N.: Mechanical characterization of Ti-added MgB_2/Cu superconducting wires using Vickers hardness test. Mater. Chem. Phys. **101**, 470–474 (2007)
36. Sergius, A., Liao, X.Y., Zhu, Y.T., Coulter, J.Y., Huang, J.Y., Willis, J.O., Peterson, D.E., Mueller, F.M., Moreno, N.O., Thompson, J.D., Indrakanti, S.S., Nesteronko, V.F.: The influence of microstructures and crystalline defects on the superconductivity of MgB_2. J. Appl. Phys. **92**, 351 (2002)
37. Vanderbemden, Ph., Bradley, A.D., Doyle, R.A., Lo, W., Astill, D.M., Cardwell, D.A., Campbell, A.M.: Physica C **302**, 257 (1998)
38. Dimos, D., Chaudhari, P., Mannhart, J.: Phys. Rev. B **41**, 4038 (1990)
39. Gielisse, P.J., Niculescu, H., Roy, B., Jones, K.W., Larkin, G., Hu, Z.: Supercond. Sci. Technol. **4**, 416 (1991)
40. Perez, F., Obradors, X., Fontcuberta, J., Bozec, X., Fert, A.: Physica C **235–240**, 2941–2942 (1994)
41. Bean, C.P.: Phys. Rev. Lett. **8**, 250 (1962)
42. Niculescu, H., Gielisse, P.J.: IEEE Trans. Magn. **28**, 809 (1992)